

DOI: 10.1002/elan.201800474

Point-of-Care Smartphone-based Electrochemical Biosensing

Alexander C. Sun^[a] and Drew A. Hall^{*[a]}

Abstract: Point-of-care (PoC) biosensors offer promising solutions to today's adverse and costly healthcare issues by moving diagnostic tools closer to the patient. The ubiquity of smartphones has brought about an emergence of PoC devices, which leverage the smartphone's capabilities, enabling the creation of low-cost and portable biosensors. Electrochemical biosensors are well suited for PoC testing since the transducers can be miniaturized and inexpensively fabricated. This review paper discusses recent developments in smartphone-based electrochemi-

Keywords: Smartphone · electrochemical biosensor · point-of-care

cal biosensors for PoC diagnostics. These peripherals utilize the various connectivity options (for example proprietary ports, audio headphone-jack, or wireless radio) to offload functionality to the smartphone. The smartphone-based implementations of various electrochemical techniques, such as amperometry, potentiometry, and impedance spectroscopy are explored. Major challenges include reducing power, area, and cost of measurement circuitry, while maintaining adequate performance for PoC diagnostic applications.

1 Introduction

Based on the most recent data from 2015, chronic illnesses, such as heart disease, stroke, and diabetes, are the leading cause of death and disability in the United States, with over 50% of the population having at least one chronic illness [1–3]. Furthermore, 87% of total annual healthcare expenditures (\$2.7 trillion in total) are for chronic diseases with 35% of this spending for a disproportionate 8.7% of the population [1]. The high death rate and financial cost exist even though in many cases these diseases are preventable or manageable with proper equipment. On the other hand, in lower-income countries, communicable disease, such as respiratory infections, human immunodeficiency virus (HIV), Malaria, and tuberculosis (TB) are a much larger concern and among the top causes of death [4]. Outbreaks of acute infectious disease are also a major concern as they not only can create a large death toll but also spread to other parts of the world if unchecked, such as the Ebola virus outbreak in 2014 that infected individuals in 10 different countries, caused 11,310 verified deaths, and cost \$3.6 billion dollars to control [5,6]. Much like the issues in developed countries, these diseases are often also preventable or treatable, but, in this case, the lack of adequate healthcare infrastructure makes such solutions infeasible.

A promising solution to these problems in both developing and developed countries is to use point-of-care (PoC) biosensors, as shown in Figure 1, which augments the current healthcare system by allowing for diagnostic tools to be brought closer to the patient providing more rapid and frequent feedback loops [7,8]. With PoC devices located near a patient such as with at-home diagnostics or wearables, the patient can be more involved in their own health to help prevent serious issues and manage chronic

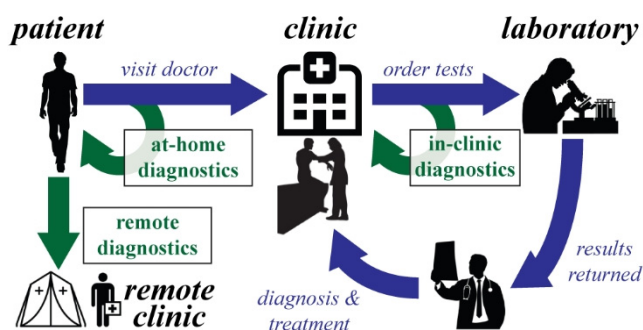


Fig. 1. Proposed concept for modern healthcare system augmented with PoC biosensors.

conditions. More comprehensive testing equipment also can be carried by the physician or placed in the doctor's office for faster results, which can lead to earlier treatment and less reliance on testing at centralized laboratories. Finally, the same technology can also be used for rapid and accurate *ad hoc* testing in remote settings. However, for these PoC platforms to be portable enough to be useful, they need to be sensitive, compact, and low-power, all qualities in line with the World Health Organization's ASSURED criteria to evaluate PoC devices [9,10].

Fortunately, as of early 2018, 68% of the world's population use mobile phones [11]. In the United States, the number of people with a mobile phone has grown to 95% with 77% specifically using a smartphone [12]. This

[a] A. C. Sun, D. A. Hall
Electrical and Computer Engineering, University of California
in San Diego, La Jolla, CA
E-mail: drewhall@ucsd.edu

growth can also be seen in other regions of the world such as Africa, Asia Pacific, and the Middle East that account for 80% of all new mobile phone subscriptions [13]. This overwhelming data clearly shows that mobile phones and, increasingly so, smartphones have become a ubiquitous part of everyday life around the world. Having what is essentially a powerful, portable, and network connected device available to a majority of the world presents a tremendous opportunity to leverage this technology to develop PoC biosensors that hold promise for portable and convenient diagnostic testing [14–16].

Hence, there has recently been a large influx of biosensing peripheral modules that attach to smartphones to take advantage of their widespread availability, computing power, network connectivity, battery, and camera to offload as much of the biosensor as possible onto the phone itself [17–20]. The goal by doing so is to create a more streamlined device that takes up less area and is less expensive compared to an equivalent stand-alone biosensor when combined with an already available smartphone. It is worth noting here that, while much of the smartphone-based biosensor ecosystem consists of optical based sensing that uses the camera for microscopy [21–30], colorimetric [31–38], and spectroscopic [39–42] assays, the following sections will only focus on electrochemical sensing. These optical techniques are typically limited by the resolution and focus of the smartphone camera as well as ambient lighting conditions [43]. On the other hand, electrochemical measurement has the advantage of being mostly independent of the smartphone's capabilities while still achieving a comparable or better formfactor than optical peripherals.

The electrochemical cell formed from electrodes submerged in an electrolytic solution is the basis of an electrochemical sensor [44, 45]. Typically, a circuit called a potentiostat is used to probe the cell by applying a stimulus voltage or current waveform between two

electrodes while simultaneously measuring the resulting current or voltage waveform at the same electrodes. For measurements that apply voltage and record current for example, any change in the cell that causes accumulation of charged molecules or promotes reduction and oxidation reactions will produce a change in the measured current, since the electrical characteristics of the cell have been altered. Electrochemical biosensors are essentially electrochemical cells with an added “bioelement,” a particularly chosen molecule (e.g., DNA, antibody, protein, peptide, etc.) whose specificity is used to isolate and detect the analyte (target molecule). The electrode or transducer converts this detection of the analyte into an electrical signal that can be measured [46]. For example, imagine that one of the electrodes, known as the working electrode (WE), has single-stranded DNA (ssDNA), the “bioelement”, immobilized on its surface meant to target its complimentary strand. When the WE is exposed to a solution full of a variety of other different ssDNA, ideally only those strands complimentary to the bound ones will combine and stick to the surface. DNA is negatively charged, so the WE has accumulated a significant amount of charge. By using the potentiostat to apply a stimulus between the WE and the other electrode called the reference electrode (RE), a difference in current will be measured between the response before and after the ssDNA was bound.

A simplified version of the potentiostat circuit is shown in Figure 2 with a third electrode, counter electrode (CE) used together in feedback with the RE to eliminate current following into the RE to reduce voltage errors [45]. The electrochemical cell itself can be modelled in terms of a network of passive electrical components (Figure 2) that is known as Randles equivalent circuit [47]. The model consists of various impedances to represent the different electrochemical phenomena that occur within the cell. As shown in Figure 2, a variety of



Alexander C. Sun received his B.S. degree (2012) in Electrical Engineering and Computer Science from the University of California, Berkeley, his M.S. degree (2014) and his Ph.D. degree (2018) in Electrical and Computer Engineering from the University of California at San Diego. His research focus is on electrochemical biosensors, electrochemical measurement techniques, and compact, low power circuit design for biomedical and point-of-care devices.



Drew A. Hall received the B.S. degree in computer engineering with honors from the University of Nevada, Las Vegas, NV, USA, in 2005, and the M.S. and Ph.D. degrees in electrical engineering from Stanford University, Stanford, CA, USA, in 2008 and 2012, respectively. From 2011 to 2013, he was a Research Scientist in the Integrated Biosensors Laboratory at Intel Corporation. Since 2013, he has been with the Department of

Electrical and Computer Engineering, University of California at San Diego, where he is currently an Associate Professor. His research interests include bioelectronics, biosensors, analog circuit design, medical electronics, and sensor interfaces. Dr. Hall has been an Associate Editor of the IEEE TRANSACTIONS ON BIOMEDICAL INTEGRATED CIRCUITS since 2015 and has been a member of the CICC Technical Program Committee since 2017. Dr. Hall received the First Place in the Inaugural International IEEE Change the World Competition and First Place in the BME-IDEA invention competition, both in 2009. He received the Analog Devices Outstanding Designer Award in 2011, an Undergraduate Teaching Award in 2014, the Hellman Fellowship Award in 2014, and an NSF CAREER Award in 2015. He is also a Tau Beta Pi Fellow.

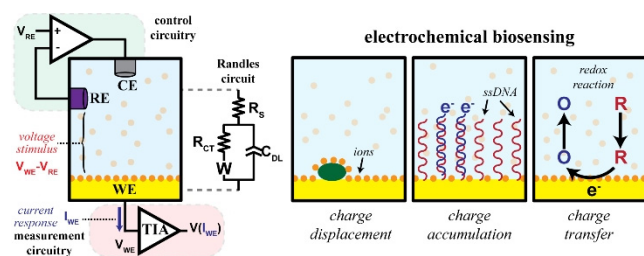


Fig. 2. Diagram of a simplified biosensor containing a potentiostat and the equivalent Randles circuit model (left). Illustration of various sensing modalities possible due to changes in the electrochemical cell (right).

different “bioelements” can affect changes in the cell such as charge displacement or accumulation, impeding or encouraging the rate of reduction/oxidation reactions, or shifting the bulk ion concentration. It is worth noting that the need for only the measurement circuitry and an electrochemically compatible electrode, which can be made from such materials as carbon, gold, silver, platinum, iridium tin oxide, or modified variants and can be fabricated down to a miniature scale ($1\ \mu\text{m}^2$ – $0.045\ \text{mm}^2$), makes electrochemical biosensors ideal for PoC applications [16,48–55]. The sensors themselves have been demonstrated to be highly scalable and can be fully integrated together with circuitry on the same chip [51,52,56–62]. While it is a nonstandard process to fabricate electrodes onto an integrated circuit or plate the top metal with a compatible material, it still typically requires fewer steps than comparable optical-based chips [63–66]. Furthermore, electrodes have also been shown to be adaptable to a variety of different point-of-care settings such as on flexible substrates or directly on the skin itself [67–69].

2 Integration with Smartphone

A number of different ways to integrate a peripheral module to a phone have been developed all with distinct trade-offs in terms of available power, data rate, and compatibility with different makes and models. For electrochemical biosensors specifically, the main functionalities that can be offloaded to the smartphone are power, two-way data transmission, stimulus generation, and signal quantization using the variety of electrical interfaces available on modern cellphones.

2.1 Wired Peripherals

2.1.1 Proprietary Interfaces

As shown in Figure 3, proprietary ports such as USB or Apple’s lightning port have been widely used both to provide power to the peripheral and to send bidirectional data [70–75]. Typically, no additional power source other than the phone is required in this case removing the hassle

of charging or replacing an extra battery, which ideally would improve patient adherence to testing. The lack of a battery also can reduce the bulkiness and size of the peripheral device. The amount of available power from these interfaces can also be relatively high with USB rated to provide a maximum of 2.5 W. This amount of power is more than enough when designing electrochemical measurement circuitry, which at most have been shown to consume 400 mW [74]. However, interfacing with these ports requires the addition of a USB interface chip (such as the CH372 or FT232R), which is essentially a component that handles the lower layer USB protocol between the phone and onboard logic [71,74]. Furthermore, compatibility between smartphone devices is limited when using only the proprietary interfaces. A device produced specifically for a certain smartphone type would need to be redesigned in order to be compatible with a different make or model. For example, a different interface would be required when switching between old and new models of the iPhone, from iPhones to Android phones, from USB-C to USB-B devices, and even between various feature phones.

2.1.1.1 USB Communication and Power

In the literature, the USB 2.0 interface has been used much more often than other wired interfaces, i.e. the lightning port on Apple devices. Several reasons for this skew exist such as Apple requiring licensing of both software and hardware in order to build a peripheral device [76] and the usage of Android phones outnumbering that of iPhones [77]. Hence, this section will focus solely on the USB interface, which uses a master-slave protocol where the host or master controls all the two-way communication between itself and multiple devices. For USB to be used between a smartphone and a peripheral device, the mobile must have the USB On-The-Go (OTG) protocol built into it and enabled by the firmware. OTG allows for the smartphone to switch between being master or slave depending on what is connected at its USB port [78]. While USB is used across a variety of different devices, whether OTG is available entirely depends on the make and model of the phone, thereby somewhat limiting its cross compatibility.

On the peripheral device itself, the physical USB connector has 4 pins, two for ground and 5 V as well as two for differential data transfer, as is standard with slave devices. The smartphone senses via this hardware connection that the peripheral is a slave and automatically provides power to the device. The USB communication protocol is strictly digital requiring that peripheral biosensors have onboard digital-to-analog converters (DAC) and analog-to-digital converters (ADC) in order to generate the correct voltage stimulus on the device and quantize the current response before transferring the results to the phone. Also, the device must implement the high level framework, packet structure, and handshake protocol discussed in many technical white papers and

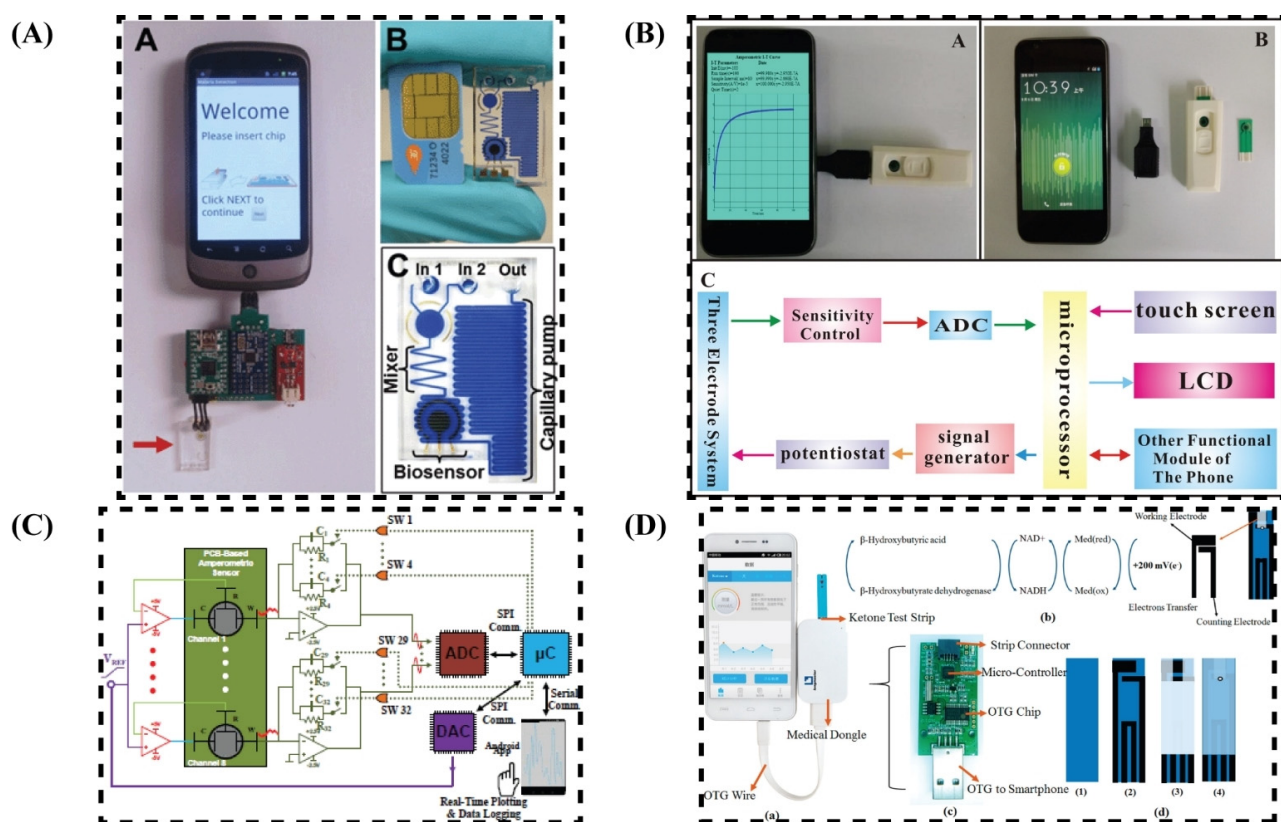


Fig. 3. Four different peripheral electrochemical biosensors that use the USB interface for data transfer and/or power. (A) A $3.5 \times 5.7 \text{ cm}^2$ sized device powered by a lithium polymer battery that transfers chronoamperometry data gathered by a Palm Instruments potentiostat to a Nexus One [70]. The platform is paired with a microfluidic electrode chip to measure a Malaria biomarker. (B) A USB powered module that uses a custom potentiostat design and screen-printed carbon electrodes [73]. (C) A $8.4 \times 5.7 \text{ cm}^2$ device that is also USB powered and has multiple channels [74]. (D) A similar biosensor module that uses a USB on-the-go chip to facilitate communication [75].

specification documents [79], by programming the microcontroller to handle queries from the host and relying on a separate USB interface chip paired with a crystal to handle the lower level data transfer. At this high level, the protocol allows for a variety of transfer types depending on the frequency, quantity of data, and amount of error correction desired. For electrochemistry, bulk transfers can be used for sending raw ADC values, while interrupt transfers can be triggered when the sensor has crossed a predefined threshold. Overall, the USB port is a widely used and familiar interface that offers both well-defined data transfer and plenty of power. However, these devices have limited cross compatibility when compared to other interfaces to be discussed.

2.1.2 Audio Headphone Port

As demonstrated in Figure 4, the 3.5-mm audio port intended for headphones can be used as an interface between a peripheral device and mobile phone. This port allows for both bidirectional data transfer via the microphone terminal and one of the output channels (left or right ear) and power transfer from the phone using the

remaining output channel. When used as the interface for power and communication for a peripheral device, the headphone jack's main advantages are that it is both the only truly universal I/O port that exists on all smartphones and has remained entirely unchanged throughout many generations of smart devices (except for the iPhone X, which requires an adapter). Hence, peripherals that use the headphone jack are essentially hardware compatible with all devices that have a three terminal audio port including laptops, tablets, mp3 players, and older mobile phones. Similar to devices that use the proprietary ports, taking power from the audio jack means that no battery other than phone's is required. However, since this port is AC coupled (bandpass from 20 Hz to 22 kHz) to prevent damaging headphones, no DC signals can pass through requiring both rectification of the audio output for power and modulation/demodulation of control and data signals.

2.1.2.1 Power Harvesting

As is demonstrated in prior art, an output sinusoid from the audio channel can be rectified with a MOSFET H-Bridge and Schottky diode to obtain a 1.2–4 V signal that

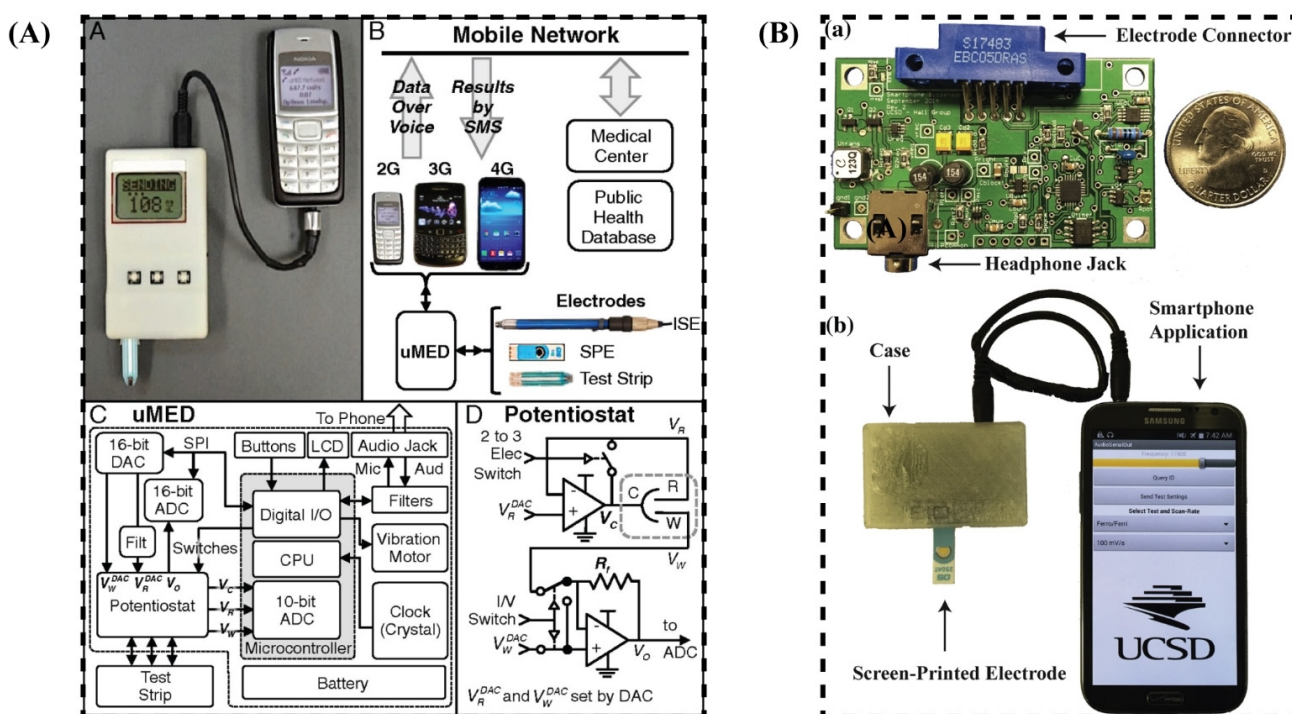


Fig. 4. Two peripheral biosensors that transmit assay result data via the audio headphone port. (A) The first device quantizes the measurements on-board and then transmits the signal digitally to the mobile, which then transmits the data over an audio phone call [87]. (B) The second can harvest power from the headphone port and is able to conduct two-way communication between the peripheral and the phone [86]. By frequency modulating the analog output signal from the potentiostat, the data can be quantized on the phone side via the microphone port.

can be further regulated and filtered [43,80–85]. However, since various makes and models of smartphones use different drivers, the output characteristics of the headphone jacks can vary. Figure 5(A) shows the measured values of both the output resistance and available power for a wide variety of smartphones. The resistances and maximum power available range from 1–20 Ω and 3–80 mW, respectively. The variation in output resistances can negatively affect the matching between the phone and the power harvesting circuitry leading to further reduced power. To account for this, a tunable matching network, such as the one shown in Figure 5(B), can be added to the peripheral device in order to change the input impedance of the harvester and improve overall power transfer efficiency. This technique has been demonstrated to improve efficiency from 52% up to 85.4% [83,86]. Even with this improvement, however, the power consumption of biosensors that use the audio port must still be low enough in order to remain compatible with most smartphones. As a result, all the peripherals in this space consume the least power (2.5–6.9 mW) when compared to other smartphone-based biosensors, aside from those that use NFC [80,82,86].

2.1.2.2 Data Transfer

Signal transmission via the audio port can be accomplished in a number of different ways as shown in Figure 6. Frequency shift keying (FSK) at ~ 17 bps handled by an on-board microcontroller can facilitate digital transmission between the smartphone and peripheral device as is demonstrated by Nemiroski et al. and Sun et al. [81,87]. Wang et al. [88] reported a phase-locked loop (PLL) (TI CB4046B) with active filters to demodulate a frequency signal from the smartphone to a voltage ramp stimulus for the potentiostat to run cyclic voltammetry. Another PLL is used to modulate the output of the potentiostat back to a frequency signal to transmit it to the phone to be quantized. This design does not require an onboard DAC, ADC, or microcontroller, instead off-loading most of this functionality to the smartphone. However, the ability to set the test parameters including scan rate and voltage range is limited because the absolute voltage and slope of the ramp are dependent on each other. In Sun et al. [86], bidirectional data was instead handled by a low power microcontroller sending and receiving UART packets in order to set the test parameters for cyclic voltammetry. The ramp signal was then generated on-board using a PWM generator and integrator with feedback to a coarse ADC to ensure accuracy. The output of the potentiostat was then converted into a frequency by a 555-timer-based voltage-controlled oscill-

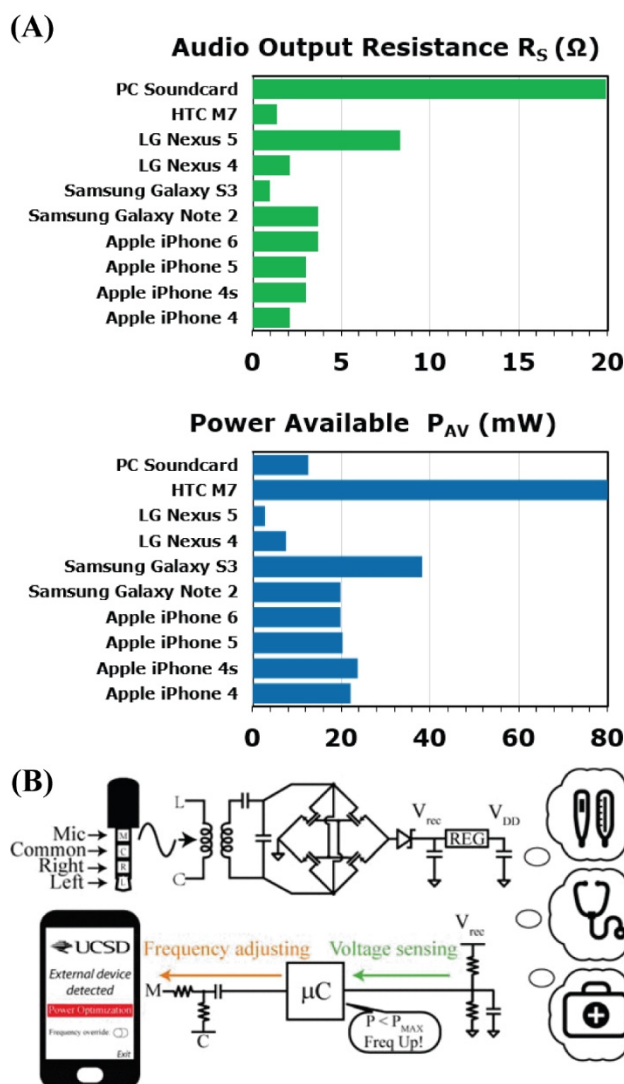


Fig. 5. (A) A survey of the headphone port output resistance and power available for a set of popular smartphones. (B) Simplified schematic of typical power harvesting circuitry with transformer, full-wave rectifier, and linear regulator. Also shown is a diagram of the automatically tunable matching network to improve power transfer efficiency [83].

lator (VCO) modulated with marker tones to ensure that the measured data lines up with the stimulus voltage. This frequency signal was then sent to the phone to be quantized. This design is able to independently set the voltage range and scan rate, while still consuming low enough power to be powered off of the audio jack. Jiang et al., similar to Wang et al., completely does away with using a microprocessor, instead relying on frequency and voltage modulation of the audio output channel along with frequency and amplitude detection circuits to control the impedance biosensor [82]. This design allows the peripheral to achieve a low 2.5 mW maximum power consumption and power itself directly from the audio port.

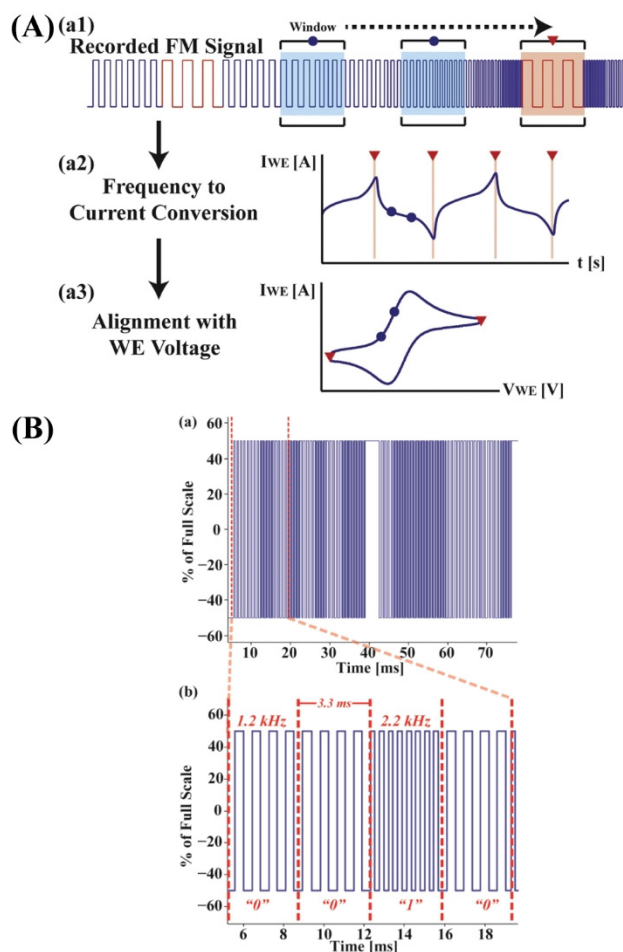


Fig. 6. Modulated (A) analog signals using a voltage-controlled oscillator and (B) digital signals using frequency shift keying transferred from a peripheral device to a smartphone [86].

In general, audio port-based peripherals offer almost universal cross compatibility at the cost of lower available power and more complicated analog circuitry compared to USB implementations. Unfortunately, while ports on the smartphone are currently widely available, we believe that in the future smartphones could move completely towards wireless interfaces making any wired peripherals obsolete in these newer models. Hence, wireless interfaces are a promising future technology for these dongles.

2.2 Wireless Peripherals

One of the main benefits of wireless schemes, i.e. Bluetooth and NFC, is that the electronics can be separate from the actual electrodes themselves, an especially important advantage in wearable-based biosensing systems where the sensor is intended to be placed directly on or near the body enabling long-term monitoring. While the topic of designing the wearable component in these platforms will not be expanded upon here because the breadth of discussion on wearables is extensive and outside the scope of this paper, one can find several

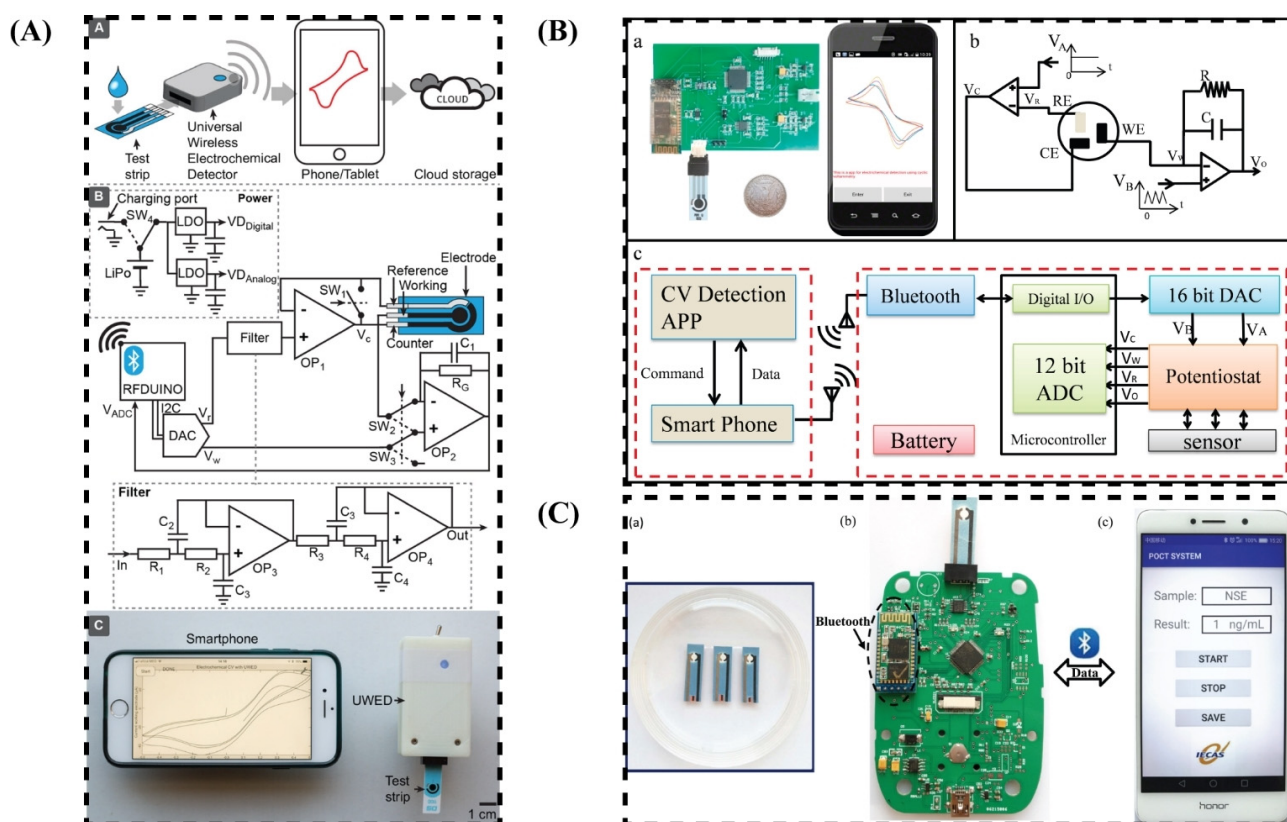


Fig. 7. Various battery powered peripherals that use Bluetooth for communication. (A) “UWED” platform uses the RFDUINO to manage the Bluetooth communication and consumes 20 mW with a size of $8 \times 4 \text{ cm}^2$ to run amperometric techniques [104]. Both (B) an $5.338.4 \text{ cm}^2$ module that specially runs differential pulse voltammetry [98] and (C) a device for cyclic voltammetry of size $11 \times 7 \text{ cm}^2$ use the HC-06 shield for handling the wireless protocol [97].

detailed and high-quality review papers about the subject [89–94]. Hence, these wireless systems can take advantage of the many advances that have been made in the effort to improve the wearability and convenience of electrochemical sensors.

2.2.1 Bluetooth

Recently more and more peripherals have begun using Bluetooth to wirelessly transmit data to and from the smartphone, as seen in the examples in Figure 7 [17,95–105]. The obvious benefit is that these types of peripherals are compatible with all types of smartphones regardless of the make or model. Also, since some companies have been shifting towards replacing most wired interfaces with wireless ones, using Bluetooth connection appears to be more future proof than the headphone port. Companies creating commercial potentiostats have also embraced Bluetooth technology as a universal method to connect to the smartphone for portable use. The EmStat Blue (PalmSens) is a battery powered and Bluetooth potentiostat capable of running a variety of electrochemical techniques. The 8 V voltage range and large current measurement range (1 nA–100 mA, 1 pA resolution) make it a good replacement for the traditional bulky

general-purpose benchtop potentiostat in many cases. The isolated wireless potentiostat from Pinnacle, Inc. is another battery powered (9 V) Bluetooth potentiostat with a smaller voltage range (4 V) and current range (80 μA) than that of the EmStat, but with two channels. However, all these wireless dongle devices require a battery that must be either replaced or recharged in addition to the smartphone’s increasing the weight and size of the device. Along with an extra battery and Bluetooth radio module with antenna (such as HC-06, HM-10, TI CC2541, Bluegiga WT-12), these types of peripherals must also generate all the voltage stimulus signals as well as quantize the potentiostat output on-board. In this way, platforms that use Bluetooth are similar to standalone biosensors and only leverage the smartphone as a readout tool.

2.2.2 NFC

Alternatively, NFC-based peripherals, such as those shown in Figure 8, also create a wireless data link between the sensor and smartphone, albeit at a much shorter distance, while also transmitting a small amount of power. The absence of a battery as well as the simplified measurement circuitry required to meet power constraints

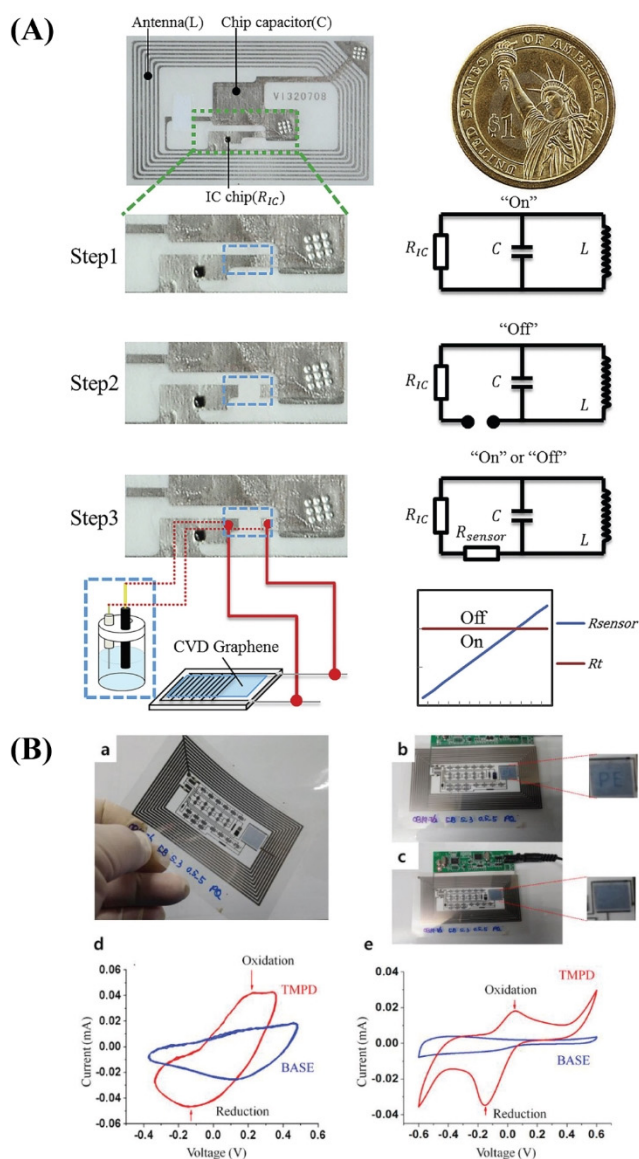


Fig. 8. Two examples of NFC tag biosensors. (A) Sensor is in parallel with antenna and detection of analyte changes its impedance thereby modulating backscatter when measured with an NFC reader [107]. (B) Tag that uses the power from NFC to run cyclic voltammetry with on-board signal generation. Readout is through an electrochromic device [110].

in this scheme enables much smaller device sizes. Often these types of platforms are created by modifying custom flexible RFID tags with a sensing film in series or shunt with the antenna and simply relying on an impedance change caused by detection of the analyte to modulate the backscatter [106–109]. Alternatively, Jung et al. reported an NFC-based biosensor that implements cyclic voltammetry using circuits made from fabricated single walled carbon nanotube network based thin film transistors [110]. This design rectifies the signal from the antenna to power a five-stage ring oscillator that generates the triangular voltage waveform applied to the modified electrodes. The

output current after amplification and buffering is applied to an electrochromic device that visually changes color when the signal surpasses a certain threshold. Hence, this architecture only provides binary detection of an analyte and does not transfer any data back to the smartphone.

The ability to receive power wirelessly allows for the dongle that performs the sensing to be generally much smaller when compared to Bluetooth modules. However, the reduced available power and inability to run when not near a reader limit the use of NFC to specific low-power and low data rate applications where size is the most important factor.

2.3 Internal Dedicated Hardware

While most smartphone-based biosensors are meant to be external peripheral devices in order to take advantage of the already saturated mobile phone market, there have been a couple of examples of modules meant to be integrated into the internal hardware of the phone as shown in Figure 9. The desired advantage in this case is that no device additional to the smartphone needs to be managed by the user, which should improve convenience and portability. However, due to the ever decreasing size and available power of modern smartphones, any devices

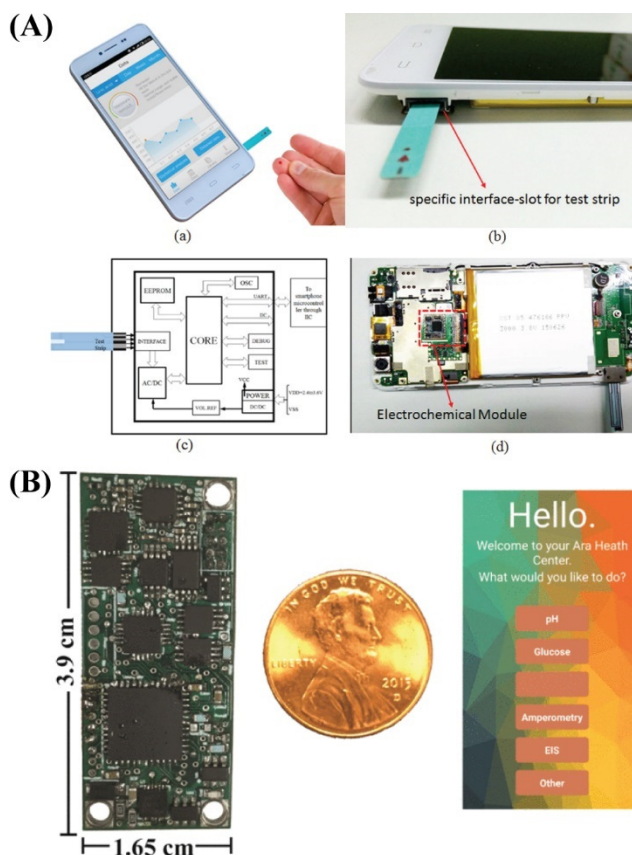


Fig. 9. Photographs of PoC biosensors (A) integrated into the hardware of a smartphone [112] and (B) as a swappable module for a modular phone [111].

integrated internally, especially noncrucial components, must be implemented in a much smaller formfactor and consume an inconsequential amount of power relative to that of other smartphone functions. For example, in terms of power, smartphones typically have a lithium-ion battery with capacity of approximately 1,500 mAh with idling and a phone call consuming 108 mW and 540 mW, respectively [111].

Guo et al. demonstrates an electrochemical measurement module integrated into a smartphone through an internal interface for power and communication [112]. Similar in design to previously discussed external electrochemical dongles but with a small enough formfactor to fit within the limited space inside the phone, this module contains a discrete ADC, DAC, voltage reference, and microcontroller, which communicates to the smartphone via I²C. However, this configuration requires access to and understanding of the inner workings of the phone, both hardware and firmware, that often are proprietary and not openly available to third-party developers. While Guo has this knowledge for this specific smartphone, this implementation is more a proof of concept to demonstrate integrating electrochemical modules into the smartphone for possible future development. This module also connects to disposable electrochemical test strips via a slot near the edge of the phone and runs an amperometric measurement technique for the detection of uric acid.

Sun et al. reports an electrochemical sensing module as well but intended for use in a modular phone specifically for the Google Ara Project [111]. Modular smartphones allow and encourage the end user to customize the functionality of their mobile device by swapping in various types of hardware modules. This 3.9 × 1.65 cm² biosensor module with a max power consumption of 100 mW contains a reconfigurable, multi-technique potentiostat that repurposes components among three different measurement modes, amperometric, potentiometric, and impedance spectroscopic. These multiple electrochemical techniques allow for varying assays to be run making the inclusion of a single biosensor module worth the space and power consumed. However, while both Guo's and Sun's approaches eliminate the need for a separate external hardware dongle, they suffer from a major limitation when compared to the devices that use other interfaces. Since these designs are intended for a particular smartphone, they are not compatible across different makes and models unlike other wired or wireless interfaces discussed. Also, the smartphone manufacturers and designers need to allow and be a part of the incorporation of the electrochemical module for these schemes to be practical.

3 PoC Implementations of E-Chem Techniques

While the interface used by a smartphone-based biosensor sets the available resources for the system, the potentiostat design determines the measurement techniques that can be run and the achievable sensitivity. A potentiostat

circuit similar to the standard transimpedance amplifier (TIA) or current conveyor based designs [56, 113–129], is used to run electrochemical techniques that require potential control and current measurement such as cyclic voltammetry, chronoamperometry, and pulse voltammetry each with its own drawbacks and advantages. The technique chosen typically depends on the application as well as the type of assay. The measurement circuitry must be able to apply a stimulus potential signal between the WE and RE that can be any combination of triangle, square, step, pulse, or sinusoidal waveforms. The applied voltage range is traditionally limited to below 1 V with a resolution of at least 5 mV. The resulting generated current waveform is then measured, which corresponds to the amount of the biomarker detected by the sensor. The signal portion of the waveform is highly dependent on the assay, concentration range of the analyte, and size of the transducer. For the PoC screen-printed electrodes or microelectrodes such signal currents can range anywhere from femtoamperes to microamperes on top of background currents so both sensitivity and dynamic range are crucial parameters. Furthermore, the bandwidth requirements typically range from sub-Hz levels to 100 kHz, so contending with 1/*f* noise for some techniques is crucial, while for others extending the bandwidth is necessary, thus integrating more noise. Therefore, in the following sections, various potentiostat implementations designed for a specific measurement mode are discussed. Table 1 summarizes and compares these smartphone-based electrochemical biosensors sorted by interface and the electrochemical techniques they can run.

3.1 Amperometry

For potential controlled current measurement techniques such as chronoamperometry (step input), cyclic voltammetry (triangular waveform input), and pulse voltammetry (pulse train input), most devices either use a commercially available AFE i.e., TI LMP91000 [130], or a custom potentiostat circuit. The advantage of LMP91000 is that the entire AFE is completely integrated into a single chip housed in a 4 × 4 mm² package that consumes ~40 μW. The detectable current range for this chip is 5–750 μA, which is acceptable for applications such as blood glucose measurement where the analyte concentration is generally high [105], but not sensitive enough for many other assays. Instead, when power can be traded for lower noise and smaller input bias current, custom potentiostat circuits with resistive feedback transimpedance amplifiers (R-TIA) are designed to obtain a higher current resolution. The open source “CheapStat” potentiostat has a current resolution of 1 nA with tunable gain from 33–165 kΩ [96, 113]. Fan et al. demonstrates a custom Bluetooth potentiostat that also achieves a current resolution of 1 nA and limit-of-detection (LOD) for neuron-specific enolase of 22 pM using differential pulse voltammetry (DPV) [97]. Sun et al. obtains a ~300 pA current resolution with a LOD for secretory leukocyte protease

Table 1. Comparative summary of smartphone-based electrochemical biosensors.

Interface	Technique	Resolution	Power Source	Power [mW]	Dimensions [cm ²]	Analyte	LOD [nM]	Ref.
USB	CA	–	lithium	–	3.5 × 5.7 (20)	PfHRP2	0.267	[70]
	Pot.	–	USB	–	–	α -amylase	89	[71]
	CV	–	USB	–	–	creatinase kinase, transaminase	35.3, 7.14	[72] "
Audio Jack	CA	–	USB	–	–	clenbuterol	0.274	[73]
	CA	–	USB	–	–	β -hydroxybutyrate	1,000	[75]
	CA	122 pA	USB	50	8.4 × 9.3 (78)	hydrogen peroxide	~	[74]
	CA	500 pA	lithium	40.7	5.6 × 11 (59)	glucose	500,000	[87]
	SWASV	"	"	"	"	heavy metal	61	"
	Pot.	"	"	"	"	sodium	–	"
	CA	"	"	"	"	PfHRP2	1	"
	CV	–	9 V	–	–	nitrate	3	[88]
	CV	300 pA	audio	6.9	3.8 × 6.4 (24)	SLPI	1.41	[86]
	Pot.	3.6 mV	audio	6.2	3.8 × 5.8 (22)	pH	–	[81]
Bluetooth	EIS	–	audio	2.5	8.1 × 6.6 (53)	NeutraAvidin	–	[82]
	CV	1,000 pA	9 V	–	–	honey	–	[96]
	CV	–	battery	–	5.3 × 8.4 (45)	glucose	26,000	[98]
	CV	–	battery	–	–	white blood cell	–	[102]
	CA	400 pA	lithium	–	5.9 × 3.3 (19)	Ru(III)Cl	–	[99]
	CA	6,400 pA	lithium	20	8 × 4 (32)	ferro/ferri	–	[104]
	CA	–	lithium	–	1.8 × 1.9 (3.4)	Glucose	–	[105]
	DPV	1,000 pA	battery	–	11 × 7 (77)	neuron-specific enolase	0.022	[97]
	EIS	–	battery	–	–	E. Coli	–	[17]
	EIS	–	battery	–	–	2,4,6-trinitrotoluene	709	[95]
NFC	EIS	–	battery	–	–	acetone	26,900	[100]
	EIS	–	lithium	–	10 × 8 (80)	blood cell	–	[101]
	EIS	–	battery	–	–	ferro/ferri	–	[103]
	Imp.	–	wireless	–	4.5 ² (20)	VCO	–	[106]
	Imp.	–	wireless	–	0.25 ² (0.06)	biogenic amines	–	[108]
	Imp.	–	wireless	–	4.1 × 2.4 (9.8)	ethenol	22,000	[107]
	"	"	"	"	"	KCl	9,000,000	"
	CV	–	wireless	–	9.5 × 5.5 (52)	TMPD	20,000	[110]
	CA	–	internal	–	–	uric acid	–	[112]
	CV	1,000 pA	internal	111	3.9 × 1.7 (6.4)	lactoferrin	0.0125	[111]
CA	"	"	"	"	glucose	–	"	
EIS	"	"	"	"	NeutraAvidin	10	"	
Pot.	61 μ V	"	"	"	pH	–	"	

CV – cyclic voltammetry; Pot. – potentiometric; CA – chronoamperometry; SWASV – square-wave anodic stripping voltammetry; EIS – electrochemical impedance spectroscopy; Imp. – impedance measurement; DPV – differential pulse voltammetry, VCO – volatile organic compounds; TMPD – tetramethyl-p-phenylenediamin

inhibitor (SLPI) of 1.4 nM using CV in an audio-jack powered peripheral. Jung et al. and Pechlivanidis et al. also both report current resolutions for their Bluetooth based biosensors of 400 pA and 122 pA, respectively [74, 99].

3.2 Potentiometry

Potentiometric measurement circuitry typically only requires an amplifier with a large input impedance to measure the voltage from an ion selective electrode known for its high resistance (10 M Ω –1 G Ω). In Zhang et al., a USB powered non-inverting amplifier with an input bias current of ~20 nA is used and can achieve a LOD for α -amylase of 89 nM [71]. There also exists a commercial potentiometric measurement chip, i.e. LMP91200 [131], which is essentially an ultra-low leakage

buffer (600 fA), that has been used in audio-jack biosensors [81].

3.3 Electrochemical Impedance Spectroscopy

Electrochemical impedance spectroscopy (EIS) is typically measured by applying a small sinusoidal voltage stimulus between electrodes and measuring the magnitude and phase of the resulting current signal at multiple frequencies in order to calculate an impedance spectrum. Due to the typical frequency range 1–100 kHz and the low 5-mV peak amplitude of the stimulus signal, EIS tends to be the most power consumptive measurement technique since it needs to measure both magnitude and phase accurately from a small current signal at all frequencies within the spectrum. Hence, most of the PoC oriented EIS sensors require power sources such as a 9 V lithium ion

battery. As is true with the other two measurement modes, there exists a popular commercial IC solution, AD5933 [132], which is able to fit a complete digital signal generator (DDS) core, DAC, ADC, and discrete Fourier transform (DFT) hardware into a single small chip as is shown in Figure 10(A) [17,95,100]. However, the main issues with this IC are that the smallest potential stimulus it can apply is ~ 200 mV peak-to-peak and the bias point cannot be set independently of the amplitude. In most cases, EIS measurements need to be fitted to a linear impedance model. With a high stimulus amplitude, it can no longer be assumed that the data matches this linear model. Furthermore, in assays where there are redox reactions, setting the bias point accurately is crucial to the measurement. Custom EIS circuits have been created to obtain more accurate results that use on-board ADCs, DACs, and microcontrollers relying on separate batteries to provide enough power [101,103]. However, Jiang et al., as illustrated in Figure 10(B), shifts the generation of the stimulus signal and quantization to the smartphone through the headphone jack, negating the need for a microcontroller and mixed-signal circuits allowing for a very low power (2.5 mW) EIS peripheral, which is mostly analog, albeit with a frequency range limited to the audio band [82].

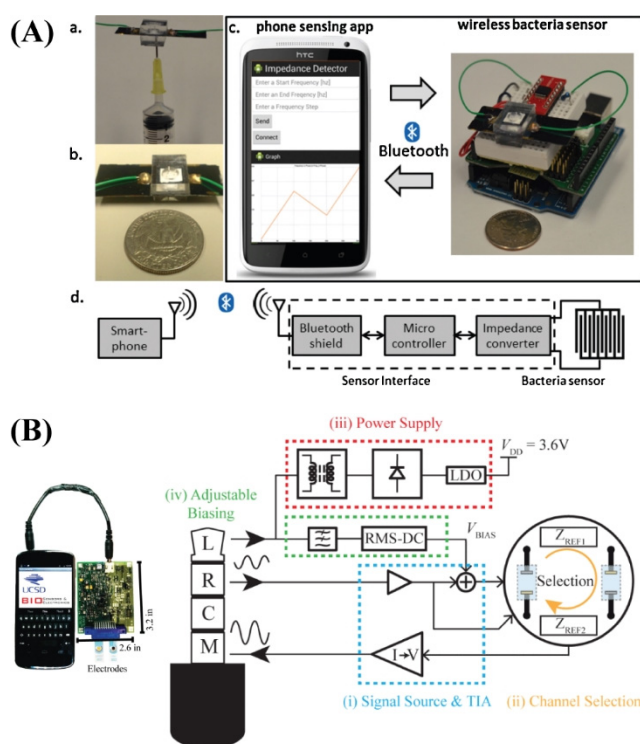


Fig. 10. PoC EIS implementations. (A) Bluetooth-based device uses an impedance converter that has on-board signal generation and Fourier transform capability [17]. (B) Audio-jack peripheral uses the output of the audio channel as the stimulus signal and relies on the microphone on the smartphone to quantize the output [82].

3.4 Multi-technique

Combining multiple techniques into a single platform allows users the versatility to run a variety of different assays all just by changing the type of electrode. Nemirski et al. successfully demonstrates a peripheral device that runs multiple amperometric and potentiometric techniques all with the same handheld-sized device paired with a mobile-phone using the headphone jack for data transfer at a rate of 17 bps [87]. The device contains a custom designed potentiostat with a current resolution of 0.5 nA along with an on-board microcontroller, 16-bit ADC, and 16-bit DAC all powered by a 3.7 V lithium polymer battery with a 210 mAh capacity. The module consumes at most 40.7 mW, and the board's dimensions are 5.6×10.6 cm². It runs chronoamperometry for detection of glucose, cyclic voltammetry for measuring *P. falciparum* (PfHRP2), square-wave anodic stripping voltammetry for heavy metal detection, and potentiometry for sodium measurements in urine. The device also has a vibration motor to increase metal deposition during stripping voltammetry thereby amplifying the electrochemical signal. Sun et al., as discussed in a previous section, also has a custom potentiostat with a 0.5 nA current sensitivity that takes up only a fraction (10%) of the area and consumes slightly more power (49.5 mW in amperometric and 111 mW in impedance spectroscopic modes) [111]. This device manages to implement cyclic voltammetry for measuring lactoferrin for urinary tract infections, chronoamperometry for blood glucose, potentiometric for pH of sweat, and impedance spectroscopy for a label-free NeutrAvidin assay.

4 Conclusion and Outlook for Future

The current ecosystem of smartphone-based PoC electrochemical biosensors was explored and the different types of interfaces were compared to demonstrate the trade-offs of each. Overall, compatibility with smartphones, amount of available power, whether an external power source is required, and the sensitivity and capabilities of the potentiostats were examined. It is worth noting here that it is often difficult to get FDA approval for smartphone-based devices since smartphones themselves are not permitted for medical use. Many commercial devices have gotten around this by not using the phone in the critical path and only having it display information. However, more and more platforms are being approved by the FDA that utilize different components of the smart device giving us hope that biosensors based off the technology discussed in this paper can one day become actual medical devices. Some examples of devices that have received approval are the Dip.io (Healthy.io), which is the smartphone-based urinalysis kit that uses the third-party smartphone camera to measure the color change on a dipstick and the KardiaBand (AliveCor), a personal EKG that is the first medical device accessory for the Apple Watch.

In terms of interfaces, there seems to be more and more wireless Bluetooth-based peripheral devices being developed and published compared to wired versions that use proprietary ports or the audio-jack. This trend is due to many factors including the increased popularity of other Bluetooth connected peripherals such as wireless headphones and credit card readers and the availability of low-power commercial off the shelf Bluetooth shields that greatly simplify making a biosensor wireless. However, many Bluetooth implementations do not improve upon the formfactor or convenience of their wired counterparts due to the inclusion of an external battery and the need for on-board signal generation.

On the other hand, NFC-based sensors appear to be one of the more promising interfaces for future development of smartphone-based biosensors that deserve further attention. It allows for power transfer from the phone to greatly reduce the size of the device while maintaining the convenience of wireless. However, the available power is miniscule (<1 mW), so innovative designs that either use passive sensing techniques or low power integrated circuit potentiostats are the clear next steps in this space. Eventually, the sensing circuit could be fully mounted on the electrode itself without needing any additional external hardware.

Furthermore, while each type of peripheral biosensor has its own advantages and optimal use cases, carrying around multiple dongles for different PoC assays is burdensome. Hence a device that combines all the techniques and benefits together into a single biosensing platform integrated into a smartphone would greatly improve the practicality of PoC biosensors. However, since the modular smartphone has yet to be realized, the only possibility for full integration is directly interfacing with the internal hardware of standard smartphones. For this to be possible, a platform that can run multiple techniques must be significantly miniaturized. Hence, the next steps for a multi-technique smartphone-based biosensor module would be to shrink down the analog-front-end and mixed signal circuitry, typically constructed from discrete components, into an integrated circuit version, which would be much smaller and more suitable for installing inside a regular non-modular smartphone. Furthermore, there is already an extensive amount of prior art on designing integrated potentiostats that contain the analog front-end, quantizers, and digital control on a single silicon chip. These devices can outperform their discrete counterparts with pA level sensitivities and low power consumption in the μ W range [133–139]. Hence, on the electronic technology side, there is a relatively low barrier of entry to be able to incorporate one of these high-performance IC potentiostat designs into a smart device such as a smartphone, tablet, or smartwatch. However, to justify the high cost required to fabricate application specific integrated circuits and make these platforms financially viable, there needs to be a high amount of consumer interest in them as well as enough validated and proven biosensing applications that hope-

fully will be accomplished using this current generation of smartphone-based biosensors. It is our hope that these further improvements will promote the use of specialized, portable, and practical medical devices well positioned to be the first line of defense in the future of healthcare.

Acknowledgements

This work was supported in part by Google's Advanced Technologies & Projects (ATAP), the US Agency for International Development (grant #AID-OAA-A-13-00002), and the National Institutes of Health, Grant UL1TR000100. The content is solely the responsibility of the authors and does not necessarily represent the official views of the NIH.

References

- [1] B. W. Ward, J. S. Schiller, R. A. Goodman, *Prev. Chronic. Dis.* **2014**, *11*.
- [2] S. Murphy, J. Xu, K. Kochanek, S. Curtin, E. Arias, *Deaths: Final Data for 2015*, National Center For Health Statistics (U.S.). Division Of Vital Statistics, **2017**.
- [3] *Health, United States, 2016 With Chartbook on Long-Term Trends in Health*, National Center For Health Statistics (U.S.). Centers For Disease Control And Prevention, **2017**.
- [4] *Global Health Estimates 2016: Deaths by Cause, Age, Sex, by Country and by Region, 2000–2016*, World Health Organization, Geneva, **2018**.
- [5] D. Gatherer, *J. Gen. Virol.* **2014**, *95*, 1619–1624.
- [6] H. A. Shiwani, R. B. Pharithi, B. Khan, C. B.-A. Egom, P. Kruzliak, V. Maher, E. E.-A. Egom, *Asian Pac. J. Trop. Med.* **2017**, *10*, 6–10.
- [7] E. Petryayeva, W. Russ Algar, *RSC Adv.* **2015**, *5*, 22256–22282.
- [8] L. Bueno, W. R. de Araujo, T. R. L. C. Paixão, in *Med. Biosens. Point Care POC Appl.* (Ed.: R.J. Narayan), Woodhead Publishing, **2017**, pp. 183–201.
- [9] G. Wu, M. H. Zaman, *Bull. W. H. O.* **2012**, *90*, 914–920.
- [10] P. K. Drain, E. P. Hyle, F. Noubary, K. A. Freedberg, D. Wilson, W. R. Bishai, W. Rodriguez, I. V. Bassett, *Lancet Infect. Dis.* **2014**, *14*, 239–249.
- [11] “Digital in 2018: World’s internet users pass the 4 billion mark,” can be found under <https://wearesocial.com/blog/2018/01/global-digital-report-2018>, **2018**.
- [12] *Pew Res. Cent. Internet Sci. Tech* **2018**.
- [13] K. Barboutox, “Key figures – Ericsson Mobility Report,” can be found under <https://www.ericsson.com/en/mobility-report/reports/november-2017/key-figures>, **2017**.
- [14] M.-P. Gagnon, P. Ngangue, J. Payne-Gagnon, M. Desmartis, *J. Am. Med. Inform. Assoc.* **2016**, *23*, 212–220.
- [15] C. Jenkins, N.-S. Burkett, B. Ovbiagele, M. Mueller, S. Patel, B. Brunner-Jackson, R. Saulson, F. Treiber, *mHealth* **2016**, *2*.
- [16] S. Nayak, N. R. Blumenfeld, T. Laksanasopin, S. K. Sia, *Anal. Chem.* **2017**, *89*, 102–123.
- [17] J. Jiang, X. Wang, R. Chao, Y. Ren, C. Hu, Z. Xu, G. L. Liu, *Sens. Actuators B Chem.* **2014**, *193*, 653–659.
- [18] D. Quesada-González, A. Merkoçi, *Biosens. Bioelectron.* **2017**, *92*, 549–562.
- [19] A. Roda, E. Michelini, M. Zangheri, M. Di Fusco, D. Calabria, P. Simoni, *TrAC Trends Anal. Chem.* **2016**, *79*, 317–325.

- [20] J. Hu, X. Cui, Y. Gong, X. Xu, B. Gao, T. Wen, T. J. Lu, F. Xu, *Biotechnol. Adv.* **2016**, *34*, 305–320.
- [21] D. N. Breslauer, R. N. Maamari, N. A. Switz, W. A. Lam, D. A. Fletcher, *PLoS One* **2009**, *4*, e6320.
- [22] L. Guan, J. Tian, R. Cao, M. Li, Z. Cai, W. Shen, *Anal. Chem.* **2014**, *86*, 11362–11367.
- [23] M. K. Kanakasabapathy, H. J. Pandya, M. S. Draz, M. K. Chug, M. Sadasivam, S. Kumar, B. Etemad, V. Yogesh, M. Safavieh, W. Asghar, *Lab Chip* **2017**, *17*, 2910–2919.
- [24] S. A. Lee, C. Yang, *Lab Chip* **2014**, *14*, 3056–3063.
- [25] X. Meng, H. Huang, K. Yan, X. Tian, W. Yu, H. Cui, Y. Kong, L. Xue, C. Liu, S. Wang, *Lab Chip* **2016**, *17*, 104–109.
- [26] I. Navruz, A. F. Coskun, J. Wong, S. Mohammad, D. Tseng, R. Nagi, S. Phillips, A. Ozcan, *Lab Chip* **2013**, *13*, 4015–4023.
- [27] D. Tseng, O. Mudanyali, C. Oztoprak, S. O. Isikman, I. Sencan, O. Yaglidere, A. Ozcan, *Lab Chip* **2010**, *10*, 1787–1792.
- [28] H. Zhu, O. Yaglidere, T.-W. Su, D. Tseng, A. Ozcan, *Lab Chip* **2011**, *11*, 315–322.
- [29] Q. Wei, H. Qi, W. Luo, D. Tseng, S. J. Ki, Z. Wan, Z. Göröcs, L. A. Bentolila, T.-T. Wu, R. Sun, *ACS Nano* **2013**, *7*, 9147–9155.
- [30] Z. J. Smith, K. Chu, A. R. Espenson, M. Rahimzadeh, A. Gryshuk, M. Molinaro, D. M. Dwyre, S. Lane, D. Matthews, S. Wachsmann-Hogiu, *PLoS One* **2011**, *6*, e17150.
- [31] S. Cho, A. Islas-Robles, A. M. Nicolini, T. J. Monks, J.-Y. Yoon, *Biosens. Bioelectron.* **2016**, *86*, 697–705.
- [32] F. Giavazzi, M. Salina, E. Ceccarello, A. Ilacqua, F. Damin, L. Sola, M. Chiari, B. Chini, R. Cerbino, T. Bellini, *Biosens. Bioelectron.* **2014**, *58*, 395–402.
- [33] S. C. Kim, U. M. Jalal, S. B. Im, S. Ko, J. S. Shim, *Sens. Actuators B Chem.* **2017**, *239*, 52–59.
- [34] E. Lebiga, R. E. Fernandez, A. Beskok, *Analyst* **2015**, *140*, 5006–5011.
- [35] V. Oncescu, D. O'Dell, D. Erickson, *Lab Chip* **2013**, *13*, 3232–3238.
- [36] A. Roda, M. Guardigli, D. Calabria, M. M. Calabretta, L. Cevenini, E. Michelini, *Analyst* **2014**, *139*, 6494–6501.
- [37] L. Shen, J. A. Hagen, I. Papautsky, *Lab Chip* **2012**, *12*, 4240–4243.
- [38] A. K. Yetisen, N. Jiang, A. Tamayol, G. U. Ruiz-Esparza, Y. S. Zhang, S. Medina-Pando, A. Gupta, J. S. Wolffsohn, H. Butt, A. Khademhosseini, *Lab Chip* **2017**, *17*, 1137–1148.
- [39] D. Gallegos, K. D. Long, H. Yu, P. P. Clark, Y. Lin, S. George, P. Nath, B. T. Cunningham, *Lab Chip* **2013**, *13*, 2124–2132.
- [40] H. Guner, E. Ozgur, G. Kokturk, M. Celik, E. Esen, A. E. Topal, S. Ayas, Y. Uludag, C. Elbuken, A. Dana, *Sens. Actuators B Chem.* **2017**, *239*, 571–577.
- [41] X. Wang, T.-W. Chang, G. Lin, M. R. Gartia, G. L. Liu, *Anal. Chem.* **2017**, *89*, 611–615.
- [42] Y. Wang, X. Liu, P. Chen, N. T. Tran, J. Zhang, W. S. Chia, S. Boujday, B. Liedberg, *Analyst* **2016**, *141*, 3233–3238.
- [43] S. Choi, *Biotechnol. Adv.* **2016**, *34*, 321–330.
- [44] Allen J. Bard, Larry R. Faulkner, *Electrochemical Methods Fundamentals and Applications*, Wiley, **2001**.
- [45] J. Wang, *Analytical Electrochemistry*, John Wiley & Sons, Inc., **2006**.
- [46] N. J. Ronkainen, H. B. Halsall, W. R. Heineman, *Chem. Soc. Rev.* **2010**, *39*, 1747–1763.
- [47] J. E. B. Randles, *Discuss. Faraday Soc.* **1947**, *1*, 11–19.
- [48] M. Hu, I. Fritsch, *Anal. Chem.* **2015**, *87*, 2029–2032.
- [49] K. Ino, Y. Kanno, T. Nishijo, H. Komaki, Y. Yamada, S. Yoshida, Y. Takahashi, H. Shiku, T. Matsue, *Anal. Chem.* **2014**, *86*, 4016–4023.
- [50] C. Ma, N. M. Contento, P. W. Bohn, *J. Am. Chem. Soc.* **2014**, *136*, 7225–7228.
- [51] B. Nasri, T. Wu, A. Alharbi, M. Gupta, R. RanjitKumar, S. Sebastian, Y. Wang, R. Kiani, D. Shahrjerdi, in *IEEE Int. Solid-State Circuits Conf.*, **2017**, pp. 268–269.
- [52] D. A. Hall, J. S. Daniels, B. Geuskens, N. Tayebi, G. M. Credo, D. J. Liu, H. Li, K. Wu, X. Su, M. Varma, in *IEEE Int. Solid-State Circuits Conf.*, **2016**, pp. 288–289.
- [53] A. Hassibi, T. H. Lee, in *IEEE Int. Pap. Solid-State Circuits Conf.*, **2005**, pp. 564–617 1.
- [54] B. N. Kim, A. D. Herbst, S. J. Kim, B. A. Minch, M. Lindau, *Biosens. Bioelectron.* **2013**, *41*, 736–744.
- [55] D. K. Pandey, P. Singh, J. Singh, S. Sachan, S. Srivastava, S. K. Singh, *Electroanalysis* **2016**, *28*, 2472–2488.
- [56] A. Manickam, A. Chevalier, M. McDermott, A. D. Ellington, A. Hassibi, *IEEE Trans. Biomed. Circuits Syst.* **2010**, *4*, 379–390.
- [57] M. J. Milgrew, M. O. Riehle, D. R. S. Cumming, *Sens. Actuators B Chem.* **2005**, *111–112*, 347–353.
- [58] J. Rothe, O. Frey, A. Stettler, Y. Chen, A. Hierlemann, *Anal. Chem.* **2014**, *86*, 6425–6432.
- [59] B. Lim, S. Takahashi, M. Futagawa, F. Dasai, M. Ishida, K. Sawada, in *2014 IEEE Biomed. Circuits Syst. Conf.*, **2014**, pp. 113–116.
- [60] K. Niitsu, S. Ota, K. Gamo, H. Kondo, M. Hori, K. Nakazato, *IEEE Trans. Biomed. Circuits Syst.* **2015**, *9*, 607–619.
- [61] B. C. Cheah, A. I. Macdonald, C. Martin, A. J. Streckas, G. Campbell, M. A. Al-Rawhani, B. Nemeth, J. P. Grant, M. P. Barrett, D. R. S. Cumming, *IEEE Trans. Biomed. Circuits Syst.* **2016**, *10*, 721–730.
- [62] A. C. Sun, E. Alvarez-Fontecilla, A. G. Venkatesh, E. Aronoff-Spencer, D. A. Hall, *IEEE J. Solid-State Circuits* **2018**, 1–11.
- [63] A. Hassibi, R. Singh, A. Manickam, R. Sinha, B. Kuimelis, S. Bolouki, P. Naraghi-Arani, K. Johnson, M. McDermott, N. Wood, in *IEEE Int. Solid-State Circuits Conf.*, **2017**, pp. 68–69.
- [64] L. Hong, H. Li, H. Yang, K. Sengupta, *IEEE J. Solid-State Circuits* **2017**, *52*, 2388–2406.
- [65] S. Koppa, Y. Joo, in *2013 IEEE Sens.*, **2013**, pp. 1–4.
- [66] B. Jang, P. Cao, A. Chevalier, A. Ellington, A. Hassibi, in *IEEE Int. Solid-State Circuits Conf.*, **2009**, pp. 436–437.
- [67] J. Kim, I. Jeerapan, S. Imani, T. N. Cho, A. Bandodkar, S. Cinti, P. P. Mercier, J. Wang, *ACS Sens.* **2016**, *1*, 1011–1019.
- [68] W. Gao, S. Emaminejad, H. Y. Y. Nyein, S. Challa, K. Chen, A. Peck, H. M. Fahad, H. Ota, H. Shiraki, D. Kiriya, *Nature* **2016**, *529*, 509–514.
- [69] A. Modali, S. R. K. Vanjari, D. Dendukuri, *Electroanalysis* **2016**, *28*, 1276–1282.
- [70] P. B. Lillehoj, M.-C. Huang, N. Truong, C.-M. Ho, *Lab Chip* **2013**, *13*, 2950–2955.
- [71] L. Zhang, W. Yang, Y. Yang, H. Liu, Z. Gu, *Analyst* **2015**, *140*, 7399–7406.
- [72] W. Deng, Y. Dou, P. Song, H. Xu, A. Aldalbahi, N. Chen, N. N. El-Sayed, J. Gao, J. Lu, S. Song, *J. Electroanal. Chem.* **2016**, *777*, 117–122.
- [73] Y. Dou, Z. Jiang, W. Deng, J. Su, S. Chen, H. Song, A. Aldalbahi, X. Zuo, S. Song, J. Shi, *J. Electroanal. Chem.* **2016**, *781*, 339–344.
- [74] N. G. Pechlivanidis, K. I. Papadimitriou, D. Evans, N. Vasilakis, T. Prodromakis, in *IEEE Int. Symp. Circuits Syst.*, **2017**, pp. 1–4.

- [75] J. Guo, *Anal. Chem.* **2017**, *89*, 8609–8613.
- [76] “MFi Program - Apple Developer,” can be found under <https://developer.apple.com/programs/mfi/>, **2018**.
- [77] “Mobile Operating System Market Share Worldwide,” can be found under <http://gs.statcounter.com/os-market-share/mobile/worldwide>, **2018**.
- [78] USB Implementers Forum, Inc., “USB On-The-Go and Embedded Host,” can be found under <http://www.usb.org/developers/onthego/>, **2018**.
- [79] USB Implementers Forum, Inc., “USB.org – USB 2.0 Documents,” can be found under http://www.usb.org/developers/docs/usb20_docs/, **2017**.
- [80] A. Sun, T. Wambach, A. G. Venkatesh, D. A. Hall, in *IEEE Biomed. Circuits Syst. Conf.*, **2014**, pp. 312–315.
- [81] A. Sun, T. Phelps, C. Yao, A. G. Venkatesh, D. Conrad, D. A. Hall, *Sensors* **2017**, *17*, 1245.
- [82] H. Jiang, A. Sun, A. G. Venkatesh, D. A. Hall, *IEEE Sens. J.* **2017**, *17*, 589–597.
- [83] C. Yao, A. Sun, D. A. Hall, in *IEEE Glob. Humanit. Technol. Conf.*, **2015**, pp. 219–225.
- [84] T. Phelps, H. Jiang, D. A. Hall, in *IEEE Eng. Med. Biol. Soc. Conf.*, **2017**, pp. 3297–3300.
- [85] Y. S. Kuo, T. Schmid, P. Dutta, ACM DEV '10 Proceedings of the First ACM Symposium on Computing for Development Article No. 24 London, United Kingdom – December 17–18, **2010** doi > 10.1145/1926180.1926210.
- [86] A. C. Sun, C. Yao, A. G. Venkatesh, D. A. Hall, *Sens. Actuators B Chem.* **2016**, *235*, 126–135.
- [87] A. Nemiroski, D. C. Christodouleas, J. W. Hennek, A. A. Kumar, E. J. Maxwell, M. T. Fernández-Abedul, G. M. Whitesides, *Proc. Natl. Acad. Sci.* **2014**, *111*, 11984–11989.
- [88] X. Wang, M. R. Gartia, J. Jiang, T.-W. Chang, J. Qian, Y. Liu, X. Liu, G. L. Liu, *Sens. Actuators B Chem.* **2015**, *209*, 677–685.
- [89] J. R. Windmiller, J. Wang, *Electroanalysis* **2013**, *25*, 29–46.
- [90] A. J. Bandodkar, W. Jia, J. Wang, *Electroanalysis* **2015**, *27*, 562–572.
- [91] J. Heikenfeld, *Electroanalysis* **2016**, *28*, 1242–1249.
- [92] D. Pankratov, E. González-Arribas, Z. Blum, S. Shleev, *Electroanalysis* **2016**, *28*, 1250–1266.
- [93] M. D. Steinberg, P. Kassal, I. M. Steinberg, *Electroanalysis* **2016**, *28*, 1149–1169.
- [94] A. J. Bandodkar, D. Molinnus, O. Mirza, T. Guinovart, J. R. Windmiller, G. Valdés-Ramírez, F. J. Andrade, M. J. Schöning, J. Wang, *Biosens. Bioelectron.* **2014**, *54*, 603–609.
- [95] D. Zhang, J. Jiang, J. Chen, Q. Zhang, Y. Lu, Y. Yao, S. Li, G. Logan Liu, Q. Liu, *Biosens. Bioelectron.* **2015**, *70*, 81–88.
- [96] G. F. Giordano, M. B. R. Vicentini, R. C. Murer, F. Augusto, M. F. Ferrão, G. A. Helfer, A. B. da Costa, A. L. Gobbi, L. W. Hantao, R. S. Lima, *Electrochim. Acta* **2016**, *219*, 170–177.
- [97] Y. Fan, J. Liu, Y. Wang, J. Luo, H. Xu, S. Xu, X. Cai, *Biosens. Bioelectron.* **2017**, *95*, 60–66.
- [98] D. Ji, L. Liu, S. Li, C. Chen, Y. Lu, J. Wu, Q. Liu, *Biosens. Bioelectron.* **2017**, *98*, 449–456.
- [99] J. Jung, J. Lee, S. Shin, Y. T. Kim, *Sensors* **2017**, *17*, 2416.
- [100] L. Liu, D. Zhang, Q. Zhang, X. Chen, G. Xu, Y. Lu, Q. Liu, *Biosens. Bioelectron.* **2017**, *93*, 94–101.
- [101] N. Talukder, A. Furniturewalla, T. Le, M. Chan, S. Hirday, X. Cao, P. Xie, Z. Lin, A. Gholizadeh, S. Orbine, *Biomed. Microdevices* **2017**, *19*, 36.
- [102] X. Wang, G. Lin, G. Cui, X. Zhou, G. L. Liu, *Biosens. Bioelectron.* **2017**, *90*, 549–557.
- [103] L. Yang, T. Chen, in *IEEE Biomed. Circuits Syst. Conf.*, **2017**, pp. 1–4.
- [104] A. Ainla, M. P. S. Mousavi, M.-N. Tsaloglou, J. Redston, J. G. Bell, M. T. Fernández-Abedul, G. M. Whitesides, *Anal. Chem.* **2018**, *90*, 6240–6246.
- [105] A. J. Bandodkar, S. Imani, R. Nuñez-Flores, R. Kumar, C. Wang, A. M. V. Mohan, J. Wang, P. P. Mercier, *Biosens. Bioelectron.* **2018**, *101*, 181–187.
- [106] J. M. Azzarelli, K. A. Mirica, J. B. Ravnsbæk, T. M. Swager, *Proc. Natl. Acad. Sci.* **2014**, *111*, 18162–18166.
- [107] G. Xu, Q. Zhang, Y. Lu, L. Liu, D. Ji, S. Li, Q. Liu, *Sens. Actuators B Chem.* **2017**, *246*, 748–755.
- [108] L. K. Fiddes, J. Chang, N. Yan, *Sens. Actuators B Chem.* **2014**, *202*, 1298–1304.
- [109] L. K. Fiddes, N. Yan, *Sens. Actuators B Chem.* **2013**, *186*, 817–823.
- [110] Y. Jung, H. Park, J.-A. Park, J. Noh, Y. Choi, M. Jung, K. Jung, M. Pyo, K. Chen, A. Javey, *Sci. Rep.* **2015**, *5*, srep08105.
- [111] A. Sun, A. G. Venkatesh, D. A. Hall, *IEEE Trans. Biomed. Circuits Syst.* **2016**, *10*, 945–954.
- [112] J. Guo, *Anal. Chem.* **2016**, *88*, 11986–11989.
- [113] A. A. Rowe, A. J. Bonham, R. J. White, M. P. Zimmer, R. J. Yadgar, T. M. Hobza, J. W. Honea, I. Ben-Yaacov, K. W. Plaxco, *PLoS One* **2011**, *6*, e23783.
- [114] M. Vergani, M. Carminati, G. Ferrari, E. Landini, C. Caviglia, A. Heiskanen, C. Comminges, K. Zor, D. Sabourin, M. Dufva, *IEEE Trans. Biomed. Circuits Syst.* **2012**, *6*, 498–507.
- [115] L. Li, X. Liu, W. A. Qureshi, A. J. Mason, *IEEE Trans. Biomed. Circuits Syst.* **2011**, *5*, 439–448.
- [116] S. Hwang, S. Sonkusale, Ultra Low Impedance CMOS Potentiostat for Environmental Sensing Applications, *IEEE Sensors Journal*, vol. 10, no. 4, pp. 820–821.
- [117] I. Ramfos, N. Vassiliadis, S. Blionas, K. Efstathiou, A. Fragos, C. K. O’Sullivan, A. Birbas, *Biosens. Bioelectron.* **2013**, *47*, 482–489.
- [118] C. Ionescu, P. Svasta, C. Tamas, C. Bala, L. Rotariu, in *IEEE Des. Technol. Electron. Packag. Symp.*, **2010**, pp. 215–218.
- [119] A. F. D. Cruz, N. Norena, A. Kaushik, S. Bhansali, *Biosens. Bioelectron.* **2014**, *62*, 249–254.
- [120] C.-Y. Huang, H.-Y. Lin, Y.-C. Wang, W.-Y. Liao, T.-C. Chou, in *IEEE Asia-Pac. Conf. Circuits Syst.*, **2004**, pp. 633–636 vol. 2.
- [121] C.-Y. Huang, M.-H. Lee, Z.-H. Wu, H.-Y. Tseng, Y.-C. Huang, B.-D. Liu, H.-Y. Lin, in *IEEE Circuits Syst. Int. Conf. Test. Diagn.*, **2009**, pp. 1–4.
- [122] J. R. Blanco, F. J. Ferrero, J. C. Campo, J. C. Anton, J. M. Pingarron, A. J. Reviejo, J. Manso, in *Proc. IEEE Instrum. Meas. Technol. Conf.*, **2006**, pp. 690–694.
- [123] M. M. Ahmadi, G. A. Jullien, *IEEE Trans. Circuits Syst. Regul. Pap.* **2009**, *56*, 1339–1348.
- [124] B. Goldstein, D. Kim, J. Xu, T. K. Vanderlick, E. Culurciello, *IEEE Trans. Biomed. Circuits Syst.* **2012**, *6*, 111–119.
- [125] R. G. Kakerow, H. Kappert, E. Spiegel, Y. Manoli, in *8th Int. Conf. Solid-State Sens. Actuators*, **1995**, pp. 142–145.
- [126] T. Luo, H. Wang, H. Song, J. B. Christen, in *2014 IEEE Biomed. Circuits Syst. Conf.*, **2014**, pp. 336–339.
- [127] S. M. Martin, F. H. Gebara, T. D. Strong, R. B. Brown, *IEEE Sens. J.* **2009**, *9*, 135–142.
- [128] H. S. Narula, J. G. Harris, in *Int. Symp. Circuits Syst.*, **2004**, pp. I-457–60.
- [129] R. F. B. Turner, D. J. Harrison, H. P. A. Baltes, CMOS potentiostat for amperometric chemical sensors *IEEE J. Solid-State Circuits*, (**1987**), pp. 473–478.

- [130] Texas Instruments, “Configurable AFE Potentiostat for Low-Power Chemical Sensing Applications,” LMP91000 datasheet, December **2014**.
- [131] Texas Instruments, “Integrated AFE for Low-Power pH Sensing Applications,” LMP91200 datasheet, February **2016**.
- [132] Analog Devices, “1 MSPS, 12-Bit Impedance Converter, Network Analyzer,” AD5933 datasheet, April **2017**.
- [133] M. H. Nazari, M. Mujeeb-U-Rahman, A. Scherer, in *IEEE Symp. VLSI Circuits*, **2014**, pp. 1–2.
- [134] A. Agarwal, A. Gural, M. Monge, D. Adalian, S. Chen, A. Scherer, A. Emami, in *IEEE Symp. VLSI Circuits*, **2017**, pp. C108–C109.
- [135] L. Zuo, S. K. Islam, I. Mahbub, F. Quaiyum, *IEEE Trans. Circuits Syst. II Express Briefs* **2015**, *62*, 204–208.
- [136] M. H. Nazari, H. Mazhab-Jafari, L. Leng, A. Guenther, R. Genov, *IEEE Trans. Biomed. Circuits Syst.* **2013**, *7*, 338–348.
- [137] M. Punjiya, C. H. Moon, S. S. Nanolab, in *IEEE Int. Symp. Circuits Syst.*, **2016**, pp. 2883–2886.
- [138] M. M. Ahmadi, G. A. Jullien, *IEEE Trans. Biomed. Circuits Syst.* **2009**, *3*, 169–180.
- [139] M. Razzaghpour, S. Rodriguez, E. Alarcon, A. Rusu, in *IEEE Biomed. Circuits Syst. Conf.*, **2011**, pp. 5–8.

Received: July 11, 2018

Accepted: August 23, 2018

Published online on November 26, 2018